Journal of Materials Science & Technology 103 (2022) 67–72

Contents lists available at ScienceDirect

Journal of Materials Science & Technology

journal homepage: www.elsevier.com/locate/jmst

Research Article

Effect of work hardening discrepancy on strengthening of laminated Cu/CuZn alloys

Zheng Cao[a,b,1], Zhao Cheng[a,1], Wei Xu[c], Lei Lu[a,*]

[a] Shenyang National Laboratory for Materials Science, Institute of Metal Research, Chinese Academy of Sciences, Shenyang 110016, China
[b] School of Materials Science and Engineering, University of Science and Technology of China, Shenyang 110016, China
[c] The State Key Laboratory of Rolling and Automation, Northeastern University, Shenyang 110819, China

ARTICLE INFO

Article history:
Received 10 March 2021
Revised 26 June 2021
Accepted 27 June 2021
Available online 27 August 2021

Keywords:
Laminated Cu/Cu alloys
Work hardening
Strengthening
Interfacial affected zone
Strain localization

ABSTRACT

To clarify the work hardening discrepancy effect on the strengthening of laminated metals, we designed two laminated Cu/Cu4Zn and Cu/Cu32Zn samples with different layer thicknesses. Cu/Cu4Zn has larger work hardening discrepancy between two constituent layers relative to Cu/Cu32Zn, but the yield strengths of two CuZn constituents are comparable. Uniaxial tensile results suggest Cu/Cu4Zn with larger work hardening discrepancy exhibits a significant strengthening at early deformation stage while Cu/Cu32Zn possesses a better ductility. The underlying mechanisms for the strengthening effect are attributed to more geometrically necessary dislocations accumulated at interfaces and severer strain localization due to the larger work hardening discrepancy.

1. Introduction

Laminated or multilayered materials, which can be produced through conventional deposition, plastic deformation and subsequent thermo-mechanical treatments, have been emerging as one of the most promising candidates to exhibit a superior combination of high strength, good ductility and considerable work hardening [1–5].

Previous investigations have focused on the role of the strength of constituent layer and the hetero-phase interface (or layer thickness effect) in causing the superior properties [1,6,7]. Generally, the strengthening of laminated metals is attributed to the incompatible deformation at interfaces between two different constituents or layers [1,8]. With decreasing the individual layer thickness from micrometer to nanometers, the strength of laminated materials can be increased five-to ten-fold over that of their constituents or an averaged strength of all constituents [1,2,9].

From a mechanical point of view [10–12], plastic strain gradient stemming from the deformation incompatibility between two constituents leads to the generation of geometrically necessary dislocations (GNDs) at the interfaces [13]. These GNDs contribute to the strengthening via promoting the kinematic hardening process [13–15]. The density of GNDs is essentially proportional to the plastic strain gradient [10,12,16], which closely depends on the difference in yield strength between the constituents.

In contrast to enormous studies on the strengthening and hardening mechanism of laminated materials [1,2,17,18], the ductility or work hardening analysis on their constituents in most literature is rather limited. The ductility or work hardening reflects on the uniform plastic deformability or stability during tensile loading [19], and inevitably varies counter to the yield strength in homogeneous counterparts. More importantly, ductility and work hardening ability of the constituents generally become crucial for the mechanical stability and final failure strain as well as its fracture toughness, based on the Considère-Hart necking criterion [20].

In this study, in order to clarify work hardening discrepancy effect on the strengthening of laminated metals, we designed two different sorts of laminated Cu/Cu alloy samples. Both Cu4Zn and Cu32Zn have the same yield strengths. Cu4Zn has very limited uniform elongation and almost work hardening free, while Cu32Zn exhibits uniform elongation as high as 30% and a desirable work hardening ability. By use of accumulative roll-bonding (ARB) [21] and subsequent thermal treatments, two series of Cu/Cu4Zn and Cu/Cu32Zn laminated samples with different layer thicknesses are prepared. Our experimental results show that the larger work hardening discrepancy between the two constituents has a strong strengthening effect on the early deformation stage, *i.e.*, the higher yield strength for Cu/Cu4Zn; while the high work hardening of

* Corresponding author.
E-mail address: llu@imr.ac.cn (L. Lu).
[1] These authors contributed equally to this work.

https://doi.org/10.1016/j.jmst.2021.06.043
1005-0302/

both constituents and additional strengthening at interfaces would contribute to a desirable later stage deformation, namely better ductility and higher ultimate tensile strength for Cu/Cu32Zn.

2. Experimental

Commercial pure copper (99.9%) and two commercial Cu4Zn and Cu32Zn alloys with Zn content of 4 and 32 wt.%, respectively, were used to produce the laminated Cu/Cu4Zn and Cu/Cu32Zn by the ARB technique. Prior to the ARB processes, the surfaces of individual Cu or CuZn constituents were cleaned by acetone and then brushed to remove the oxide layer and to ensure sufficient bonding. The unique ARB process in this study is in the following:

Step 1: A sandwich-like sample with 1 mm-thick Cu alloy in the core and two 0.5 mm-thick pure copper sheets in the surfaces was heated at 773 K for 8 min and then the first warm rolling was performed immediately by a thickness reduction of 50%.

Step 2: The warm-rolled sample was cooled to room temperature in order to clean the surfaces, cut and stack up again.

Then, reheat the stacked-up sample for the 2nd warm-rolling process and step 2. And so on for the 3rd, 4th and 5th ...warm rolling cycles.

Step 3: After all warm-rolling cycles, the warm-rolled sample was cold-rolled with 40% thickness reduction at room temperature, yielding the sample thickness of 600 μm.

Step 4: Finally, the rolled sample was annealed at 553 K for Cu/Cu4Zn or 563 K for Cu/Cu32Zn for 2 h, respectively, to ensure both Cu4Zn and Cu32Zn constituents possess the same yield strength.

Correspondingly, the average layer thicknesses of the cold-rolled samples after 1, 4 and 5 warm-rolling cycles become 300, 38 and 19 μm, respectively. Parallelly, to prepare the homogeneous Cu, Cu4Zn and Cu32Zn samples, the freestanding samples experienced the same ARB processes and annealing which have almost the same microstructures compared to the laminated metals.

The cross-sectional microstructures of laminated Cu/CuZn and their freestanding counterparts were examined by FEI Nova NanoSEM 460 scanning electron microscope (SEM) with backscattering electron (BSE) imaging mode. Electron backscatter diffraction (EBSD) was conducted under 20 kV with a step size of 100 nm. The measured area was 40 μm $\times$ 40 μm and the data was analyzed by channel 5^{TM} software. The kernel average misorientation (KAM) method was used to calculate the local misorientation from the EBSD orientation data. The threshold value was set as 3° beyond which the misorientation is believed to be induced by grain boundaries (GBs). The GND density was estimated by $\rho_{GND} = \frac{2\theta}{\mu b}$ [13], where μ is the unit length (100 nm) and b is the Burgers vector magnitude of Cu (0.255 nm) and θ is the local misorientation. The local misorientation of every single point was calculated based on the 24 surrounding points.

A Qness Q10A+ micro-hardness tester was employed to test the cross-sectional hardness of laminated Cu/Cu alloy samples with a load of 50 g and loading time of 10 s. The dog-bone-shaped tensile samples with 5 mm in length and 2 mm in width were cut from sheets using electrical discharge machining and polished to reduce the surface roughness. The loading direction is parallel to the rolling direction (layer interface). The uniaxial quasi static tensile tests were carried out by Instron 5848 microtester at a strain rate of 5×10^{-3} s^{-1} at room temperature. Tension strain was measured by a contactless MTS LX300 laser extensometer. At least three tensile specimens were tested for the reproducibility for each laminated or freestanding constituent sample.

The *ex-situ* digital image correlation (DIC) technique was applied to measure the strain evolution on the lateral surface of laminated materials. The speckle patterns were prepared using electrochemical etching method in a solution of 10 g $FeCl_3$, 100 mL H_2O and 2.5 mL HCl under a voltage of 0.7 V for 15 s. The lateral surface morphologies of the sample deformed at strain ε = 0, 1% and 3% were recorded using SEM with the secondary electron mode. As for these SEM images with a resolution of 124 nm/pixel, the strain distribution was analyzed using the DIC MATLAB program (Ncorr 2D) with a strain radius of 7 pixels and a step of 2 pixels.

3. Results and discussion

As designed, two series of laminated Cu/Cu4Zn and Cu/Cu32Zn samples with different layer thicknesses were fabricated. Taking the laminated samples with layer thickness λ = 19 μm as examples, we show the typical SEM images of microstructures in Fig. 1. Laminated Cu/Cu4Zn was comprised of an alternate distribution of coarse-grained (CG) Cu and ultrafine-grained Cu4Zn constituent layers (Fig. 1(a)). The magnified SEM image in Fig. 1(b) shows Cu and Cu4Zn layers are well bonded with a sharp interface. A similar laminated structure of Cu/Cu32Zn sample is shown in Fig. 1(c). The average grain sizes of Cu4Zn layer (Fig. 1(b)) and Cu32Zn layer (Fig. 1(d)) are 340 nm and 1.2 μm, respectively, both of which are comparable to those of the freestanding counterparts (Table 1). However, regardless of the much larger grain size, Cu32Zn has the same hardness (1.4 GPa) with that of Cu4Zn.

As we know, the microstructure of the rolled metals mainly depends on the cold rolling and the annealing treatment, while the effect of the warm rolling is minor. Specifically, the cold rolling strain dominates the grain size of cold-rolled sample, and the subsequent annealing temperature/time dominates the recovery of these deformed grains. Here we fixed the same cold rolling thickness reduction (40%) and the same annealing treatment (553 K 2 h for Cu/Cu4Zn and 563 K 2 h for Cu/Cu32Zn), resulting in a comparable grain size of Cu, Cu4Zn or Cu32Zn layer in the laminated samples with different layer thicknesses.

Tensile engineering stress-strain curves of freestanding Cu, Cu4Zn and Cu32Zn samples are shown in Fig. 2(a). The pure Cu sample has a yield strength of 119 MPa and a uniform elongation (30%), which is consistent with the annealing Cu sheet in the literature [1]. Cu4Zn sample exhibits a yield strength of 352 MPa but a low uniform elongation (1.5%), while Cu32Zn has a comparable yield strength (341 MPa) and larger uniform elongation (28.8%). The inset in Fig. 2(a) shows the work hardening discrepancy is huge between Cu and Cu4Zn but negligible between Cu and Cu32Zn.

It should be noted that the comparable yield strength but higher work hardening in Cu32Zn relative to Cu4Zn can be understood in terms of the grain size and Zn content. Regarding Cu32Zn, the larger grain size contributes to a lower yield strength. But the yield strength of Cu32Zn can be compensated via a stronger solid-solution strengthening induced by more Zn. Such, Cu32Zn with a larger grain size shows a comparable strength to that of Cu4Zn with a smaller grain size. In addition, the larger grain size of Cu32Zn contributes to a larger work hardening capacity by more interior dislocations activity [22]. In other words, the significant work hardening discrepancy stems from the grain size difference between the two Cu alloys.

Fig. 2(b) shows the tensile engineering stress-strain curves of laminated Cu/Cu4Zn and Cu/Cu32Zn with different layer thicknesses. Both laminated samples exhibit strong layer-thickness-dependent tensile properties. As λ decreases, the strength and ductility of both Cu/Cu4Zn and Cu/Cu32Zn increase simultaneously, which is consistent with the previous reports [1,13]. Obviously, the yield strength of Cu/Cu4Zn is higher than that of Cu/Cu32Zn when λ is constant. Still taking the samples with λ = 19 μm as examples, the yield strength of Cu/Cu4Zn (264 MPa) is higher than that of Cu/32 Zn (225 MPa). As summarized in Fig. 2(c), as λ decreases,

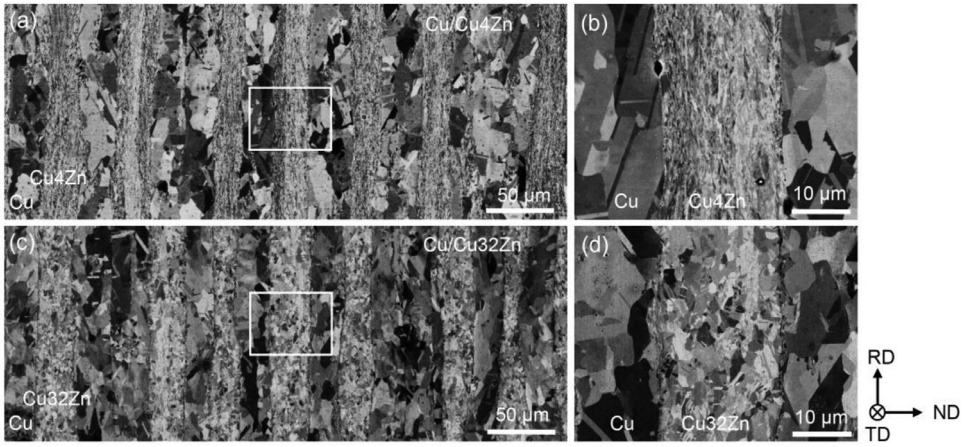

Fig. 1. Low magnification SEM images of Cu/Cu4Zn (a) and Cu/Cu32Zn (c) with layer thickness of 19 μm. High magnified SEM images of Cu/Cu4Zn (b) and Cu/Cu32Zn (d) as indicated by white boxes in (a) and (b). RD, ND and TD are rolling, normal and transverse directions, respectively.

Table 1
The average grain size, yield strength, uniform elongation and ultimate strength of laminated Cu/Cu4Zn, Cu/Cu32Zn with layer thickness of 19 μm compared to their freestanding constituents Cu, Cu4Zn and Cu32Zn.

Sample	Grain size (μm)	Yield strength (MPa)	Uniform elongation (%)	Ultimate strength (MPa)
Cu	7 ± 0.2	119 ± 6	30 ± 0.6	243 ± 3
Cu4Zn	0.32 ± 0.01	352 ± 1	1.5 ± 0.2	360 ± 2
Cu32Zn	1.7 ± 0.1	341 ± 7	28.8 ± 1.5	448 ± 1
Cu/Cu4Zn(19 μm)	7.5 ± 0.2 (Cu)0.34 ± 0.01 (Cu4Zn)	264 ± 6	13.7 ± 2.5	308 ± 2
Cu/Cu32Zn(19 μm)	4.7 ± 0.2 (Cu)1.2 ± 0.1 (Cu32Zn)	225 ± 2	29.6 ± 0.7	345 ± 2

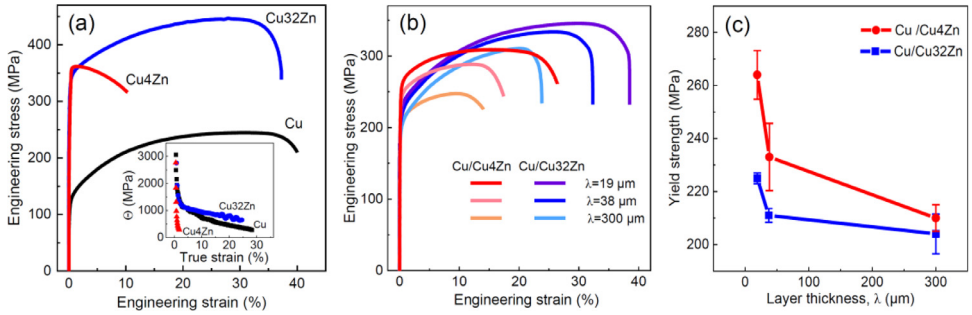

Fig. 2. Tensile engineering stress-strain curves of freestanding Cu, Cu4Zn, Cu32Zn samples (a), and laminated Cu/Cu4Zn, Cu/Cu32Zn with different layer thicknesses (b). The inset of (a) shows work-hardening rate vs. true strain of freestanding Cu, Cu4Zn, Cu32Zn. (c) The variation of yield strengths of two laminated metals with different layer thicknesses.

the yield strength of Cu/Cu4Zn increases more rapidly than that of Cu/Cu32Zn, indicating that the larger work hardening discrepancy makes for a significant strengthening at the early deformation stage. Cu/Cu32Zn has a ductility of 29.6% and the ultimate tensile strength of 345 MPa, higher than those in Cu/Cu4Zn (13.7% and 308 MPa), indicating that the higher work hardening or ductility of constituents can promote better ductility and higher ultimate tensile strength at later deformation stage.

To understand the effect of work hardening discrepancy on the strengthening effect, the microstructure evolution and GND distributions near interfaces in laminated Cu/Cu4Zn and Cu/Cu32Zn with $\lambda = 19$ μm with increasing applied strains were investigated by EBSD. As shown in Fig. 3(a), the Cu layer in Cu/Cu4Zn has a random orientation. Some small grains are intermingled among large grains in the Cu layer near the interface, indicating an incompletely recrystallized microstructure. As the tensile strain is applied to 1% (Fig. 3(b)) the microstructure has little change. These grains, especially near interfaces, are lengthened along the tensile axis after the strain of 9% (Fig. 3(c)). On the contrary, the microstructures of the Cu layer in Cu/Cu32Zn almost keep constant as the tensile strain increases from 0% to 9% (Fig. 3(d–f)). This indicates that the Cu layer will sustain a larger deformation in Cu/Cu4Zn relative to Cu/Cu32Zn.

As shown in Fig. 4(a), GND density near the interface of the as-prepared Cu/Cu4Zn is higher than that in the interiors of the Cu layer, which corresponds to the formation of the interface affected zone (IAZ) [1] during ARB process. As the applied strain increases from 1% to 9%, the GND density in IAZ is enhanced (Fig. 4(b) and (c)). On the contrary, the GND density is lower in Cu/Cu32Zn from $\varepsilon = 0\%$ to 9% (Fig. 4(d–f)). Fig. 4(g) and (h) compares the average GND distributions across Cu layers in both laminated samples. It further shows that GND densities in Cu interiors are comparable for two samples, but GND density in IAZ of Cu4Zn is higher than that in Cu32Zn, suggesting that a larger work hardening discrepancy facilitates the GND storage in the IAZ.

To further understand the effect of work hardening discrepancy, we measured the full-field strain distributions of the lateral surface of two laminated samples at the early and later stages based on DIC technique. The distribution of tensile strain, ε_{xx}, in Cu/Cu4Zn sample with $\lambda = 19$ μm deformed at early stage $\varepsilon = 1\%$ was

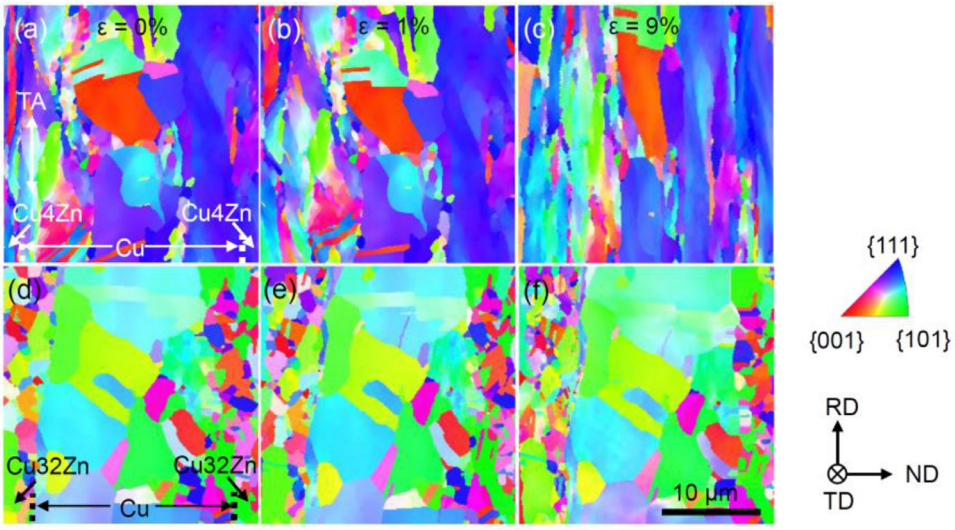

Fig. 3. Inverse pole figure mapping colored by transverse-direction (TD) of the Cu/Cu4Zn (a–c) and Cu/Cu32Zn (d-–f) samples under different tensile strains of 0% (a,d), 1% (b,e) and 9% (c,f).

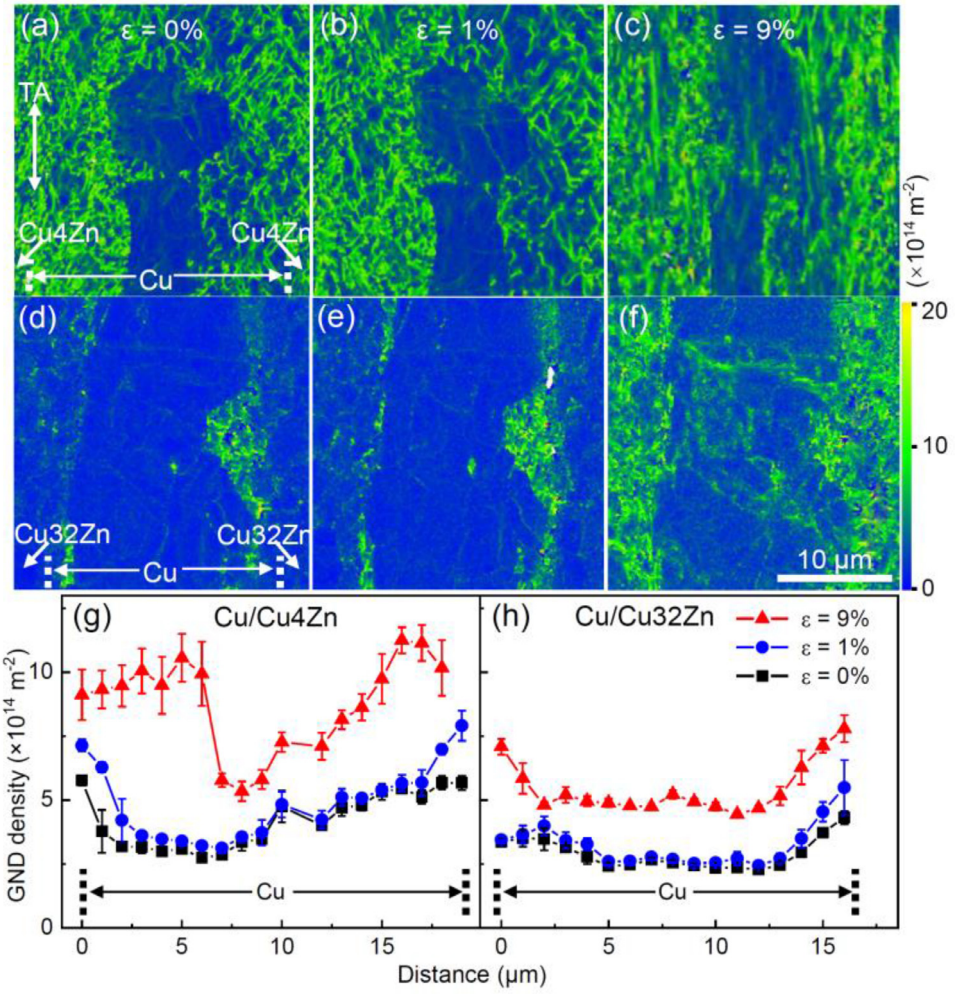

Fig. 4. GND density mapping from EBSD measurement of laminated Cu/Cu4Zn (a–c) and Cu/Cu32Zn (d–f) with layer thickness of 19 μm at ε = 0%, 1% and 9%, as indicated. Averaged GND density distributions in Cu layer at different strains of Cu/Cu4Zn (g) and Cu/Cu32Zn (h). TA, tensile axis.

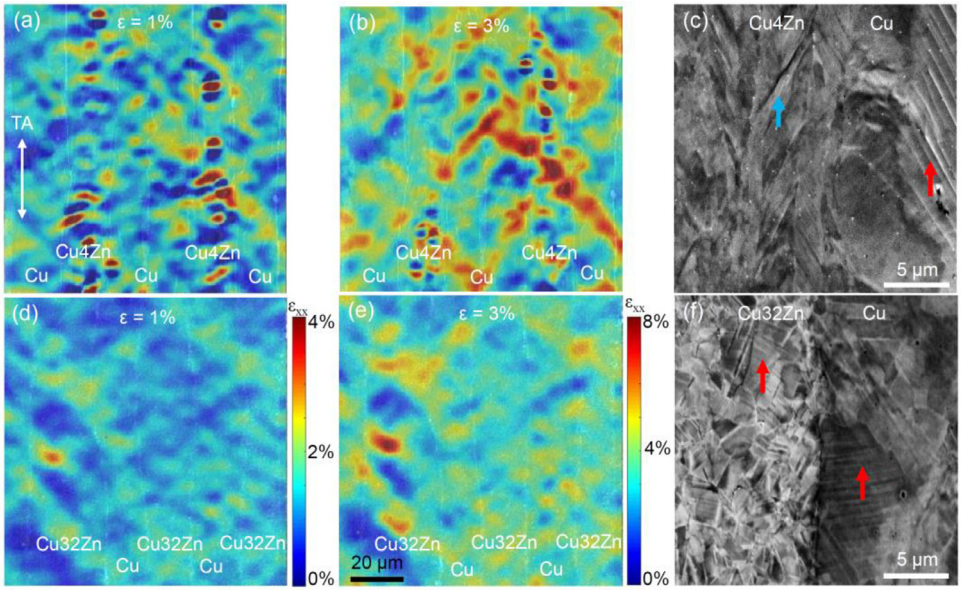

Fig. 5. Distribution of strain along tensile axis, ε_{xx}, of Cu/Cu4Zn (a,b) and Cu/Cu32Zn (d,e) with layer thickness of 19 μm at ε = 1% and ε = 3% as indicated. The deformation morphologies on lateral surface of Cu/Cu4Zn (c) and Cu/Cu32Zn (f) deformed at ε= 9%. Shear bands and slip bands are indicated by blue and red arrows, respectively.

shown in Fig. 5(a). The strain distributes very non-uniformly in Cu4Zn layers, showing obvious strain localization, as reported in previous studies [23–25]. To make a quantitative analysis, the average strain localization frequency, defined as number of strain localization regions per unit area, and average strain gradient, defined as the strain variation per unit distance across the strain localization region, will be discussed below. As the applied strain increases from 1 to 3% (Fig. 5(b)), the strain localization frequency and strain gradient in Cu/Cu4Zn increase from 373 to 421 mm^{-2} and from 1.1 to 1.4 mm^{-1}, respectively. A few severe strain localization regions are formed and penetrate into several layers. The strain localization is related to the prevailing shear bands in Cu4Zn layers, while the ubiquitous slip bands in pure Cu layers suggest homogeneous plastic deformation by dislocation gliding, as shown in Fig. 5(c).

However, the strain localization is less obvious in deformed Cu/Cu32Zn with λ = 19 μm. As displayed in Fig. 5(d) and (e), as the applied strain increases from 1 to 3%, the average strain localization frequency and strain gradient of Cu32Zn increases from 142 to 257 m^{-2} and from 0.2 to 0.22 m^{-1}, respectively, both of which are lower relative to Cu4Zn. The weaker strain localization is consistent with prevailing slip bands in both Cu and Cu32Zn as shown in Fig. 5(f).

Above experimental results clearly show that both yield strength and ductility of laminated Cu/CuZn samples also depend on the work hardening discrepancy, in addition to the layer thickness dependence. The strengthening of laminated structure is attributed to the formation of IAZ with strain gradient and GNDs accumulation at the interfaces [1,13]. As layer thickness decreases, the yield strength and ductility of laminated Cu/Cu4Zn and Cu/Cu32Zn increase simultaneously due to the increase of volume fraction of IAZs (Fig. 2).

It has been reported that the storage of GNDs at interfaces can be improved by increasing the difference of yield strength between the two adjacent constituents [6] or increasing interface strength via hard intermetallic compounds [26]. The underlying mechanism for those approaches is based on reinforcing the interfaces that can undertake higher stress or strain concentration, beneficial for more GNDs to pile up [1,13].

As for the laminated Cu/Cu4Zn, we found that the larger work hardening discrepancy between two constituents would also promote the storage of GNDs at the interfaces or IAZs (Fig. 4) and improve the strengthening at early deformation stage (Fig. 2). This can be understood in terms of the work hardening capacity or corresponding deformation mechanisms of two constituents. During deformation of Cu/Cu4Zn laminates, dislocations nucleated in Cu layer tend to be piled up at interfaces (Fig. 4(a–c)) and induce stress/strain concentration, which is hard to be released due to the limited dislocation activities in Cu4Zn layer, as proved by the abundant unstable shear bands (Fig. 5(c)). On the contrary, the dislocations piled-up induced stress/strain concentration at interfaces in Cu/Cu32Zn with high work hardening can be easily alleviated due to the sufficient activity of dislocations (indicated by dislocation bands in Fig. 5(f)) in Cu32Zn layer. Such, less GNDs storage at interfaces of Cu/Cu32Zn is seen in Fig. 4(d–f).

Strain localization at later deformation stage depends on the work hardening discrepancy between adjacent constituents as well. For example, necking or serious strain localization happens easily in freestanding Cu4Zn, but in the laminated structure, the premature necking of Cu4Zn is suppressed, resulting from strong constraint deformation between two adjacent layers [24,27]. As a result, the otherwise single strain localization region of Cu4Zn is dispersed into many tiny areas as shown in Fig. 5. Meanwhile, accompanying with the strain variation across these regions, the pronounced plastic strain gradient appears and accordingly promotes the accumulation of GNDs [28] and stress state change [24], further helping the strengthening effect.

4. Conclusion

In summary, the larger work hardening discrepancy between two constituents improves the yield strength at initial deformation stage, due to the improved GNDs storage and more serious strain localization. Moreover, the better plastic deformability of Cu/Cu32Zn is attributed to a larger work hardening of constituents and the additional strengthening induced by GNDs at the interfaces. These findings provide an additional strategy to optimize the mechanical properties of laminated metals.

Acknowledgments

The authors acknowledge financial support by the National Natural Science Foundation of China (Nos. U1608257 and 51931010),

the Key Research Program of Frontier Science and International Partnership Program (No. GJHZ2029), CAS, LiaoNing Revitalization Talents Program (No. XLYC1802026). Z. Cheng acknowledges financial support by the National Natural Science Foundatiosn of China (No. 52001312), the Project Funded by China Postdoctoral Science Foundation (Nos. BX20190336 and 2019M661150) and the Open Research Fund from the State Key Laboratory of Rolling and Automation, Northeastern University (No. 2018RALKFKT002).

References

[1] C.X. Huang, Y.F. Wang, X.L. Ma, S. Yin, H.W. Höppel, M. Göken, X.L. Wu, H.J. Gao, Y.T. Zhu, Mater. Today 21 (2018) 713–719.
[2] A. Misra, J.P. Hirth, R.G. Hoagland, Acta Mater. 53 (2005) 4817–4824.
[3] M. Göken, H.W. Höppel, Adv. Mater. 23 (2011) 2663–2668.
[4] J. Park, J.S. Kim, M. Kang, S.S. Sohn, W.T. Cho, H.S. Kim, S. Lee, Sci. Rep. 7 (2017) 40231.
[5] Y.C. Wang, X.M. Luo, L.J. Chen, H.W. Yang, B. Zhang, G.P. Zhang, J. Mater. Sci. Technol. 34 (2018) 2283–2289.
[6] Y.F. Wang, C.X. Huang, X.T. Fang, H.W. Höppel, M. Göken, Y.T. Zhu, Scr. Mater. 174 (2020) 19–23.
[7] J. Wang, Q. Zhou, S. Shao, A. Misra, Mater. Res. Lett. 5 (2016) 1–19.
[8] Y. Wang, C. Huang, Y. Li, F. Guo, Q. He, M. Wang, X. Wu, R.O. Scattergood, Y. Zhu, Int. J. Plast. 124 (2020) 186–198.
[9] I.J. Beyerlein, N.A. Mara, J.S. Carpenter, T. Nizolek, W.M. Mook, T.A. Wynn, R.J. McCabe, J.R. Mayeur, K. Kang, S. Zheng, J. Wang, T.M. Pollock, J. Mater. Res. 28 (2013) 1799–1812.
[10] M.F. Ashby, Philos. Mag. 21 (1970) 399–424.
[11] N.A. Fleck, G.M. Muller, M.F. Ashby, J.W. Hutchinson, Acta Metall. Mater. 42 (1994) 475–487.
[12] H. Gao, Y. Huang, W.D. Nix, J.W. Hutchinson, J. Mech. Phys. Solids 47 (1999) 1239–1263.
[13] X. Ma, C. Huang, J. Moering, M. Ruppert, H.W. Höppel, M. Göken, J. Narayan, Y. Zhu, Acta Mater. 116 (2016) 43–52.
[14] N.A. Fleck, M.F. Ashby, J.W. Hutchinson, Scr. Mater. 48 (2003) 179–183.
[15] Z. Cheng, H. Zhou, Q. Lu, H. Gao, L. Lu, Science 362 (2018) 559.
[16] Y. Zhang, Z. Cheng, L. Lu, T. Zhu, J. Mech. Phys. Solids 140 (2020) 103946.
[17] M.Y. Seok, J.A. Lee, D.H. Lee, U. Ramamurty, S. Nambu, T. Koseki, J.I. Jang, Acta Mater. 121 (2016) 164–172.
[18] H. Ding, X. Cui, N. Gao, Y. Sun, Y. Zhang, L. Huang, L. Geng, J. Mater. Sci. Technol. 62 (2021) 221–233.
[19] S.D. Antolovich, R.W. Armstrong, Prog. Mater. Sci. 59 (2014) 1–160.
[20] E.W. Hart, Acta Metall. 15 (1967) 351–355.
[21] I.J. Beyerlein, J.R. Mayeur, S. Zheng, N.A. Mara, J. Wang, A. Misra, Proc. Natl. Acad. Sci. U. S. A. 111 (2014) 4386–4390.
[22] M.A. Meyers, A. Mishra, D.J. Benson, Prog. Mater. Sci. 51 (2006) 427–556.
[23] M. Huang, C. Xu, G. Fan, E. Maawad, W. Gan, L. Geng, F. Lin, G. Tang, H. Wu, Y. Du, D. Li, K. Miao, T. Zhang, X. Yang, Y. Xia, G. Cao, H. Kang, T. Wang, T. Xiao, H. Xie, Acta Mater. 153 (2018) 235–249.
[24] Y. Wang, C. Huang, Z. Li, X. Fang, M. Wang, Q. He, F. Guo, Y. Zhu, Extreme Mech. Lett. 37 (2020) 100686.
[25] H. Wu, M. Huang, Q. Li, J. Wu, J. Li, Z. Wang, G. Fan, Scr. Mater. 172 (2019) 165–170.
[26] J. He, Y. Ma, D. Yan, S. Jiao, F. Yuan, X. Wu, Mater. Sci. Eng. A 726 (2018) 288–297.
[27] Q. Pan, L. Lu, Scr. Mater. 187 (2020) 301–306.
[28] F. Yuan, D. Yan, J. Sun, L. Zhou, Y. Zhu, X. Wu, Mater. Res. Lett. 7 (2018) 12–17.